


Force correlator for driven disordered systems at finite temperature

Cathelijne ter Burg and Kay Jörg Wiese 

Laboratoire de Physique de l'École Normale Supérieure, ENS, Université PSL, CNRS, Sorbonne Université, Université Paris-Diderot, Sorbonne Paris Cité, 24 rue Lhomond, 75005 Paris, France



(Received 15 March 2025; accepted 11 June 2025; published 7 July 2025)

When driving a disordered elastic manifold through quenched disorder, the pinning forces exerted on the center of mass are fluctuating, with mean $f_c = -\overline{F_w}$ and variance $\Delta(w) = \overline{F_w F_0^c}$, where w is the externally imposed control parameter for the preferred position of the center of mass. $\Delta(w)$ was obtained via the functional renormalization group in the limit of vanishing temperature $T \rightarrow 0$, and vanishing driving velocity $v \rightarrow 0$. There are two fixed points, and deformations thereof, which are well understood: The depinning fixed point ($T \rightarrow 0$ before $v \rightarrow 0$) rounded at $v > 0$, and the zero-temperature equilibrium fixed point ($v \rightarrow 0$ before $T \rightarrow 0$) rounded at $T > 0$. Here we consider the whole parameter space of driving velocity $v > 0$ and temperature $T > 0$, and quantify numerically the crossover between these two fixed points.

DOI: [10.1103/dkhl-c68t](https://doi.org/10.1103/dkhl-c68t)

I. INTRODUCTION

A. Generalities

Elastic manifolds driven in a disordered medium have a depinning transition at zero temperature. Typical examples are the motion of domain walls in magnets [1–4], contact line depinning [5], earthquakes [6,7], and the peeling of an RNA-DNA helix [8]. What these systems have in common is that they are governed by an over-damped equation of motion for the interface $u(x, t)$ which is driven through a quenched disordered medium,

$$\begin{aligned} \partial_t u(x, t) &= \nabla^2 u(x, t) + m^2[w - u(x, t)] \\ &\quad + F(x, u(x, t)) + \eta(x, t), \\ w &= vt, \quad v \geq 0. \end{aligned} \quad (1)$$

Here $w = vt$ is the externally imposed control parameter for the preferred position of the center of mass, v is the driving velocity and m^2 is the stiffness of the spring which sets a renormalization scale. (See Appendix D for a list of all notations.) The disorder forces $F(x, u)$ are short-range correlated, quenched random variables, whereas $\eta(x, t)$ is a thermal noise. Their correlations are

$$\overline{F(x, u)F(x', u')} = \delta(x - x')\Delta_0(u - u'), \quad (2)$$

$$\langle \eta(x, t)\eta(x', t') \rangle = 2T\delta(x - x')\delta(t - t'). \quad (3)$$

The equation of motion (1) can be studied via field theory. Its principle object is the *renormalized force correlator* $\Delta(w)$. $\Delta(w)$ is the zero-velocity limit of the connected correlation function of the forces acting on the center of mass $u_w = \frac{1}{L^d} \int_x u(x, t)$ [9]:

$$\begin{aligned} \Delta(w) &= \lim_{v \rightarrow 0} \Delta_v(w), \\ &= \lim_{v \rightarrow 0} L^d m^4 \langle [u_w - w][u_{w'} - w']^c \rangle. \end{aligned} \quad (4)$$

The functional renormalization group (FRG) predicts two distinct universality classes, termed *depinning* and *equilibrium*.

Equilibrium is the limit of first $v \rightarrow 0$ and then $T \rightarrow 0$, whereas depinning is the limit of first $T \rightarrow 0$ and then $v \rightarrow 0$. In both classes, $\Delta(w)$ has a cusp, and admits a scaling form

$$\Delta(w) = m^4 \rho_m^2 \tilde{\Delta}(w/\rho_m). \quad (5)$$

The characteristic scale ρ_m scales with m ,

$$\rho_m \sim m^{-\zeta}, \quad (6)$$

defining a roughness exponent ζ , distinct between depinning and equilibrium. A second difference is in the shape of $\Delta(w)$.

The function $\Delta(w)$ was measured in numerical simulations [10,11] and experiments [2,4,5,8,12]. These measurements, both in simulations and experiments, are done by moving the center of the confining potential of strength m^2 at a small driving velocity v . For *depinning*, experiments were performed in soft ferromagnets, both with short-range (SR) and long-range (LR) elasticity [4], and for DNA/RNA peeling [8]. An experiment in the equilibrium universality class is DNA unzipping [12]. In all cases, the measured force correlator $\Delta(w)$ agrees with the predictions from field theory and exactly solved models. It is rounded at a finite driving velocity.

Most of the experiments above are for zero-temperature depinning, defined such that disorder dominates over entropy and thermal fluctuations are negligible. We think of a finite driving velocity as a *perturbation* which takes us away from the critical point (4)–(5). It is not the only possible perturbation: thermal noise in Eq. (1) with temperature $T > 0$ is another one. Apart from the two limiting cases (renormalization fixed points) $T \rightarrow 0$ before $v \rightarrow 0$ (depinning), and $v \rightarrow 0$ before $T \rightarrow 0$ (equilibrium), also small deformations of these limits are well understood: For depinning, driving at a finite velocity can be accounted for by twice convoluting the zero-velocity fixed point with the response function, which leads to a rounding of the cuspy fixed point [13]. However, the equilibrium fixed point is rounded by a finite temperature, described by a *thermal boundary layer* [14,15].

The goal of this paper is to describe the crossover between these two limiting cases and to serve as a reference for signals

of either perturbation. We do this by means of numerical simulations, which at fixed m^2 are parametrized by v and T . Our results capture measurements of various quantities, such as effective forces and disorder correlations, with an emphasis on quantities that can be measured in experiments. These quantities are important because they give insight into whether an experimental or numerical setting is close to depinning, close to equilibrium or “in between,” without necessarily knowing the underlying model, or the relevant microscopic parameters. The main two features are rounding of the cuspy fixed point due to either v or T , and an additional peak due to thermal fluctuations. An example where this framework was successfully applied is Ref. [12].

B. Mean-field description

Since these questions are difficult to treat numerically for an interface, we study a single degree of freedom which can itself be interpreted as the center-of-mass of the interface. This is sometimes referred to as a *mean-field* approximation. As was clarified in Ref. [13], there are different mean-field descriptions, depending on the correlations of the effective force acting on the center of mass. To properly describe experiments, we request force correlations to have a finite correlation length. This is in contrast to the ABBM [16,17] or BFM [15,18] models, for which random forces are modeled as random walks, and for which force correlations do not decay with distance. While the latter are theoretically appealing as they are simple to solve, they do not seem to be realized in nature. Contrary to long-standing claims, even magnetic domain walls in long-range magnets, for which the avalanche size exponent is correctly given by ABBM or BFM, have decaying force correlations [4].

Denoting the center of mass of the interface by $u(t)$, the equation of motion (1) and noise correlations (2)–(3) reduce to

$$\partial_t u(t) = m^2[w - u(t)] + F(u) + \eta(t), \quad (7)$$

$$\langle \eta(t)\eta(t') \rangle = 2T\delta(t - t'), \quad (8)$$

$$\overline{F(u)F(u')} = \Delta_0(u - u'). \quad (9)$$

The first term is the force exerted by a confining well, which gets replaced by a Hookean spring with spring constant m^2 . $F(u)$ is the random pinning force, possibly the derivative of a potential, $F(u) = -\partial_u V(u)$. Specifying the correlations of $F(u)$ defines the system. Following [13] we consider forces $F(u)$ that describe an Ornstein-Uhlenbeck (OU) process driven by a Gaussian white noise $\xi(u)$:

$$\partial_u F(u) = -F(u) + \xi(u),$$

$$\langle \xi(u)\xi(u') \rangle = 2\delta(u - u'). \quad (10)$$

At small distances $u \ll 1$, the forces $F(u)$ have the statistics of a random walk, thus its microscopic limit is the ABBM model [16,17]. The microscopic force correlator decays as $e^{-|u|}$, thus at large distances $u \gg 1$ forces are uncorrelated, putting our model in the random-field (RF) universality class.

Returning to the equation of motion (7), at zero temperature and at very slow driving, most of the time the left-hand side vanishes. This condition defines the force F_w , given w ,

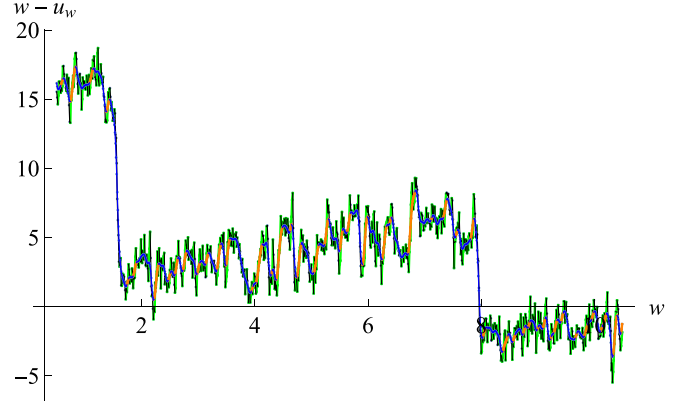


FIG. 1. $w - u_w$ for $\delta t = 10^{-3}$, $v = 0.01$, $m^2 = 0.1$, $T = 0.5$ (DNS). In green are the simulation data. The latter are then averaged over $60\delta t$. This allows us to identify forward moving sections (blue) and backward moving sections (orange).

and the associated critical force f_c as

$$F_w = m^2(u_w - w), \quad (11)$$

$$f_c := \lim_{v \rightarrow 0} -\overline{F_w} = \lim_{v \rightarrow 0} m^2 \overline{(w - u_w)}, \quad (12)$$

where u_w is the center-of-mass position of the interface¹ given w . The signs are such that exerting a positive force f_c overcomes the pinning forces $F(u_w)$. Due to the thermal noise, u_w can increase even below the threshold force by thermal activation over energy barriers U . For sufficiently small velocities, this allows the dynamics to equilibrate with activation times following an Arrhenius law $\tau \sim e^{U/T}$. Thermal fluctuations allow for u_w to go backward, violating the Middleton theorem [19] (forward-only motion at $T = 0$).

Figure 1 shows one simulation, with the original trajectory which includes all noise in green. Smoothing it over time allows us to show predominantly forward movement in blue and backward movement in orange. We see that at this temperature backward movement is substantial.

The effective disorder is defined as

$$\Delta_{v,T}(w - w') := \overline{F_w F_{w'}}^c. \quad (13)$$

We write subscripts v, T to indicate that measurements depend on both v and T . Since we have various observables and various *perturbations* ($T > 0$ or $v > 0$) we can construct a plethora of *distinct* objects. To clarify their meaning, we summarize our notations in Appendix D.

Finally, the critical force is related to the area of the hysteresis loop as

$$m^2 [\overline{(w - u_w)}^{\text{forward}} - \overline{(w - u_w)}^{\text{backward}}] = 2f_c. \quad (14)$$

Hysteresis is absent in equilibrium where $f_c = 0$ and maximal at depinning.

¹Note that for fixed $w = vt$ and $v \rightarrow 0$, the time $t \rightarrow \infty$, thus cannot be used to parametrize the interface position $u(t)$.

C. Review of known results

Before we present our findings for the questions posed in the introduction, let us review what is known for a single perturbation. Firstly, we review what happens to the *equilibrium fixed point* at a finite temperature. Secondly, we consider changes to the *depinning fixed point* induced by a finite driving velocity. These two limits are well understood.

1. Equilibrium fixed point ($v = 0$)

The zero-temperature equilibrium fixed point can be measured by energy minimization (EM) at fixed w of

$$\mathcal{H}_w(u) = \frac{m^2}{2}(u - w)^2 + V(u), \quad (15)$$

see Appendix A for implementation details. The random potential is given by $V(u) = -\int F(u)du$. For the RF disorder relevant for Eq. (10), the model is known as the Sinai model, introduced in Ref. [20]. The effective force correlator reads (see Ref. [21], with corrections in Ref. [15])

$$\Delta(w) = m^4 \rho_m^2 \tilde{\Delta}(w/\rho_m), \quad (16)$$

$$\rho_m = 2^{\frac{2}{3}} m^{-\frac{4}{3}} \sigma^{\frac{1}{3}}, \quad (17)$$

where σ sets the microscopic disorder strength.

$$\begin{aligned} \tilde{\Delta}(w) = & -\frac{e^{-\frac{w^2}{12}}}{4\pi^{\frac{3}{2}}\sqrt{w}} \int_{-\infty}^{\infty} d\lambda_1 \int_{-\infty}^{\infty} d\lambda_2 e^{-\frac{(\lambda_1 - \lambda_2)^2}{4w}} \\ & \times e^{i\frac{w}{2}(\lambda_1 + \lambda_2)} \frac{\text{Ai}'(i\lambda_1)}{\text{Ai}(i\lambda_1)^2} \frac{\text{Ai}'(i\lambda_2)}{\text{Ai}(i\lambda_2)^2} \\ & \times \left[1 + 2w \frac{\int_0^\infty dV e^{wV} \text{Ai}(i\lambda_1 + V) \text{Ai}(i\lambda_2 + V)}{\text{Ai}(i\lambda_1) \text{Ai}(i\lambda_2)} \right], \end{aligned} \quad (18)$$

where Ai is the Airy function. The roughness exponent is identified from Eq. (17) as $\zeta = 4/3$. Figure 2 shows in blue the analytical solution of Eqs. (16)–(18). In red and cyan are numerical simulations of Eq. (15) for uncorrelated forces, constant in an interval of size one, and unit variance, i.e., $\langle V(u) - V(u') \rangle \simeq |u - u'|$. Already for $m^2 = 0.01$, the simulation has converged to the theory. The inset shows comparison to the model of OU forces defined in Eq. (10), which belongs to the same universality class.

At a finite temperature, thermal fluctuations smoothen the shocks and round the cusp in a boundary layer $u \sim T$. This *thermal rounding* is shown in Fig. 3. The size of the boundary layer can be estimated from the FRG [15] (see Appendix B)

$$\Delta_T^{\text{eq}}(\tilde{w}) = \mathcal{A}_T \Delta^{\text{eq}}(\tilde{w}), \quad (19)$$

$$\tilde{w} = \sqrt{w^2 + \tilde{T}^2}, \quad \frac{\tilde{T}}{\rho_m} = \frac{3}{\varepsilon} \frac{2Tm^2}{\Delta(0)}, \quad (20)$$

$$\mathcal{A}_T = \frac{\int_0^\infty dw \Delta^{\text{eq}}(w)}{\int_0^\infty d\tilde{w} \Delta^{\text{eq}}(\tilde{w})}, \quad (21)$$

where $\Delta^{\text{eq}}(w)$ is the zero-temperature equilibrium fixed point and \tilde{T} sets the size of the boundary layer. The amplitude \mathcal{A}_T ensures normalization, i.e., that the area under $\Delta(w)$ is preserved in the presence of thermal rounding. A derivation [15] of this set of equations is given in Appendix B. Since

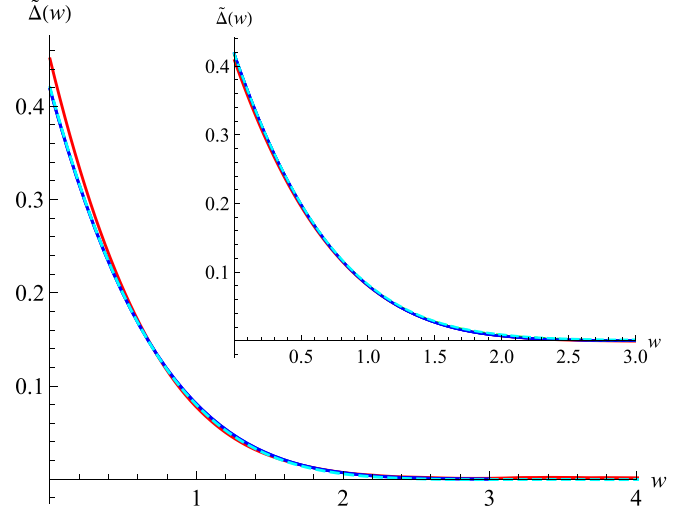


FIG. 2. $\tilde{\Delta}(w)$ for the Sinai model (blue) obtained by numerical integration of Eqs. (16)–(18). It is compared to the energy minimization for $m^2 = 0.1$ (red), $m^2 = 0.01$ (cyan dashed) indistinguishable from the theory. Statistical errors are within the line thickness. Inset: Idem for the OU model in Eq. (10).

from Eq. (20) $w \sim \tilde{T} \sim \rho_m$, the ratio \tilde{T}/ρ_m in Eq. (20) is dimensionless. This defines the dimensionless temperature $T_m \sim Tm^\theta$, scaling with its own exponent

$$\theta = d - 2 + 2\zeta, \quad (22)$$

where θ is called the *equilibrium energy exponent*. As we show in Appendix B, an alternative expression for the

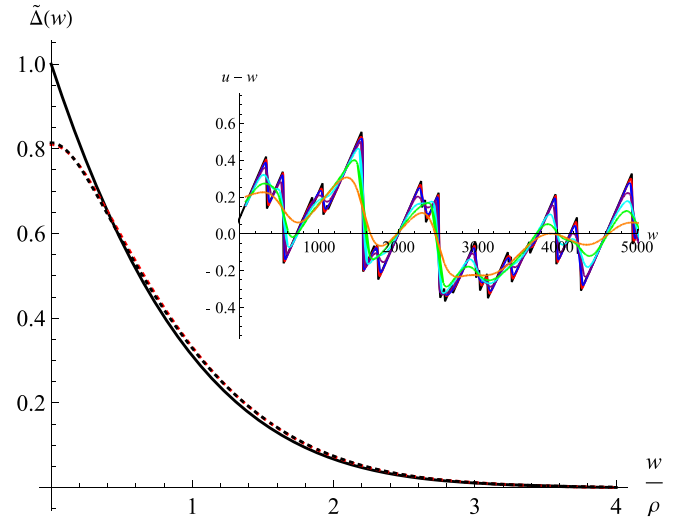


FIG. 3. Boundary layer analysis for equilibrium random-field disorder via exact minimization (EM) for the dimensionless rescaled disorder $\tilde{\Delta}(w)$ and rescaled to have unit amplitude and slope 1 at $w = 0$. Black solid, $v = 0$, $T = 0$ fixed point, black dashed, numerical measurement at $m^2 = 0.01$, $T = 2$, red dotted, thermal boundary layer ansatz using equations (19). Inset: The effective force at various temperatures: $T \in [0, 0.1, 0.2, 0.5, 1, 2, 5]$ (from black to orange), for $m^2 = 0.01$.

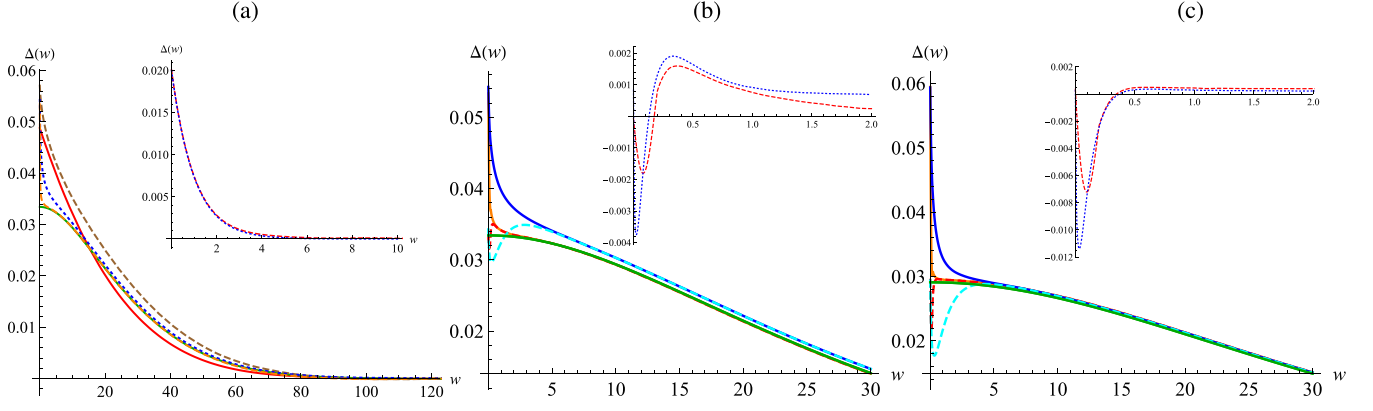


FIG. 4. (a) Inset shows a comparison of the prediction (33) for a system without disorder (blue) for $m^2 = 0.01$, $v = 10^{-3}$, $T = 2$ to a measurement of the noise correlations. Main panel (a) shows the equilibrium regime for $T = 2$ with the zero temperature fixed point $\Delta^{\text{eq}}(w)$, Eq. (16), in red and $\Delta_T^{\text{eq}}(w)$ (EM), Eq. (19), for $T = 2$ shown in green. Both are zero velocity results. Simulation of Eq. (7) shows $\Delta_{v,T}(w)$ (DNS) for $v = 0.01$ (brown), $v = 10^{-3}$ (blue) and 10^{-4} (orange). For the smallest two driving velocities the tail agreement is excellent with the zero velocity result, and the thermal peak, rounded by the driving velocity, is clearly visible. This reflects the decomposition of the amplitude in Eq. (36). The largest velocity no longer obeys the decomposition for the amplitude, Eq. (36), and belongs to the crossover regime. For the same $m^2 = 0.01$, $T = 2$ (b) and $T = 3$ (c) main panels show a zoomed in comparison of the equilibrium $\Delta_T^{\text{eq}}(w)$ [green, exact minimization (EM)] to $\Delta_{v,T}(w)$ at $v = 10^{-3}$ (blue solid, DNS) and $v = 10^{-4}$ (orange solid, DNS). In dashed cyan/red, we show the combination (35). This correctly captures the amplitude, but a signal of anticorrelations remains. In the inset we show that the corrections $\delta\Delta_{v,T}(w/v)$ introduced in Eq. (34) are small (note the scales). This subtraction is done using Eq. (33) shown in inset of panel (a).

boundary layer is given by

$$\Delta_T(w) = \int_{-\infty}^{\infty} du \Delta(u) G(u - w, \tau), \quad (23)$$

$$G(u, \tau) = \frac{1}{\sqrt{4\pi\tau}} e^{-\frac{u^2}{4\tau}}, \quad (24)$$

$$\tau = \frac{\tilde{T}^2}{\pi} - \frac{2(\pi - 2)\tilde{T}^3}{\rho_m \pi^2} + \mathcal{O}(\tilde{T}^4), \quad (25)$$

where $G(u, \tau)$ is the diffusion kernel with a fictitious time τ .

A delicate question is what the dynamical exponent z is in equilibrium. The observation that $z = 2$ in both the free theory as well as at depinning suggests that this likely holds also in equilibrium. Finally, the pinning force $f_c = 0$ in equilibrium.

2. Depinning fixed point ($T = 0$)

For depinning the effective disorder (4) is given by [13,22]

$$\Delta(w) = m^4 \rho_m^2 \tilde{\Delta}_{\text{Gumbel}}(w/\rho_m), \quad (26)$$

$$\tilde{\Delta}_{\text{Gumbel}}(w) = \frac{w^2}{2} + \text{Li}_2(1 - e^{|w|}) + \frac{\pi^2}{6}, \quad (27)$$

$$\rho_m = \frac{1}{2m^2 \ln(m^{-2})}. \quad (28)$$

Li_2 is the polylog function. The roughness exponent is $\zeta = 2^-$; the dynamical exponent is $z = 2^-$ [13]; the minus sign denotes logarithmic corrections. In the simulations, we can measure (26) at zero velocity, by moving the parabola from $w \rightarrow w + \delta w$ and waiting for the dynamics to cede. In an experiment, performed at finite v , $\Delta(w)$ is rounded by the driving velocity [13]

$$\Delta_v(w - w') = \iint_{t,t'} R(t) R(t') \Delta(w - w' - v(t - t')). \quad (29)$$

$R(t)$ is the response function in absence of disorder, decaying on a timescale $\tau = 1/m^2$,

$$R(t) = \frac{1}{\tau} e^{-t/\tau} \Theta(t). \quad (30)$$

By construction, $\int_t R(t) = 1$ and the integral of $\Delta_v(w)$ is independent of v . At small v , Eq. (29) can be approximated by

$$\Delta_v(w) = \frac{1}{\mathcal{N}} \Delta(\sqrt{w^2 + (v\tau)^2}), \quad (31)$$

where \mathcal{N} is chosen such that $\int_w \Delta_v(w) = \int_w \Delta(w)$.

For $v = 0$ the critical force f_c is defined in Eq. (12). For $v > 0$, the combination $m^2(w - u_w)$ increases to [13]

$$m^2(w - u_w) \approx f_c \Big|_{v=0} + \eta v + \mathcal{O}(v^2), \quad (32)$$

where η is the viscosity, set to $\eta = 1$ in Eq. (1).

II. RESULTS IN THE GENERAL SITUATION

We now present our numerical results, mostly obtained by direct numerical simulation (DNS). First in Sec. II A we check Eqs. (16)–(21) for equilibrium. In Sec. II B we discuss several order parameters characterizing the crossover between equilibrium and depinning. Section II C shows that with the rescalings established so far, we can collapse all our data.

A. Thermal peak in the equilibrium regime

In Fig. 4 we show the results of numerical simulations of $\Delta_{v,T}(w)$ in the near-equilibrium regime. The presence of the thermal noise leads to a thermal peak (TP) at small w . In

absence of disorder it reads

$$\begin{aligned}\Delta_v^{\text{TP}}(w - w') &= 2Tm^4 \int_{-\infty}^{\infty} R(t, \tau) R(t', \tau) d\tau \\ &= Tm^2 e^{-m^2|t-t'|} \\ &= Tm^2 e^{-m^2|w-w'|/v},\end{aligned}\quad (33)$$

where $R(t) = \Theta(t)e^{-m^2 t}$ is the response function of the free theory, and in the last line we have expressed $t - t'$ by the distance the parabola moved in this time interval. This is checked in the inset of Fig. 4(a).

Let us now turn back to the disordered case, at finite velocity $v > 0$ and finite temperature $T > 0$. We define $\delta\Delta_{v,T}(w)$ via

$$\Delta_{v,T}(w) = \Delta_T^{\text{eq}}(w) + \Delta_v^{\text{TP}}(w) + \delta\Delta_{v,T}(w). \quad (34)$$

The first term is the relevant result for $v = 0$. The second term is the contribution (33) from the thermal noise. If the driving velocity is small enough for the dynamics to equilibrate, then we expect the third term $\delta\Delta_{v,T}(t)$ to vanish, or at least to be small.

Figures 4(b) and 4(c) (insets) show the combination

$$\Delta_{v,T}(w) - \Delta_v^{\text{TP}}(w) = \Delta_T^{\text{eq}}(w) + \delta\Delta_{v,T}(w), \quad (35)$$

for $T = 2$ (b) and $T = 3$ (c). While $\Delta_v^{\text{TP}}(w)$ correctly subtracts the thermal noise at $w = 0$, the remaining term $\delta\Delta_{v,T}(t)$ is visible. In the inset, we show $\delta\Delta_{v,T}(t)$, i.e., the error we make in the approximation $\Delta_{v,T}(w) \approx \Delta_T^{\text{eq}}(w) + \Delta_v^{\text{TP}}(w)$. We see that despite a difference of v by a factor of ten, the rescaled combination $\delta\Delta_{v,T}(t = w/v)$ at small t depends little on v . This estimates the boundary layer in our example to be $\delta t \approx 2$.

Equation (34) approximately predicts the amplitude for equilibrium as

$$\Delta_{v,T}(0) \approx \Delta_T(0) + m^2 T. \quad (36)$$

As can be seen in main Fig. 4(a), this relation breaks down for $v = 0.01$, corresponding to $\hat{T} = Tm^{2/3} \ln(v) \approx 2$ and the brown dashed curve. A look at Fig. 5, discussed next, shows that there $f/f_c \approx 0.05$, which signals the approach to the crossover regime.

B. Order parameters

1. Mean force as an order parameter

The measured pinning force

$$f := m^2(w - u_w) - v, \quad (37)$$

vanishes in equilibrium, and is maximal for depinning at temperature zero, where it takes the value f_c , see Eqs. (11)–(12). It is a natural candidate for an order parameter. We define

$$\Psi_f := \frac{f}{f_c}, \quad (38)$$

which vanishes in equilibrium and is 1 at depinning. The inset of Fig. 5 shows this force ratio for different m^2 , T , and v , for $v = 0.1, 10^{-2}, 10^{-3}, 10^{-4}$, $m^2 = 10^{-3}$. Using that the dimensionless temperature is Tm^θ and velocity and temperature are related by Arrhenius' law as $\ln(v) \sim 1/T$, a natural ansatz for

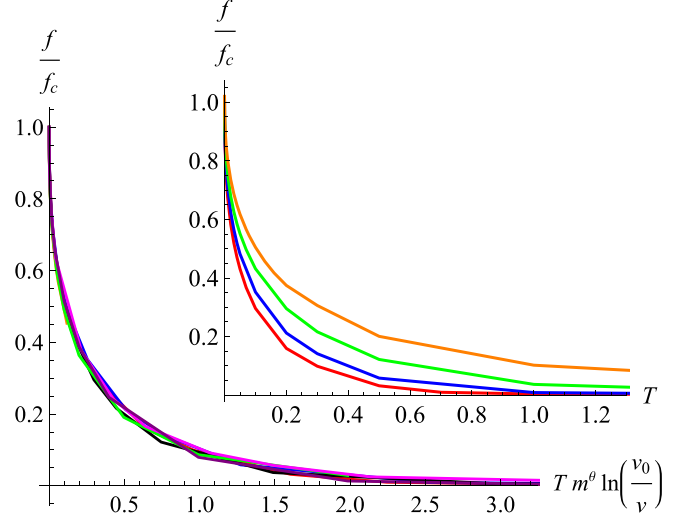


FIG. 5. Scaling collapse of the measured force for $T > 0$, and different m, v . We found an optimal collapse for $v_0 = 1$, but any v_0 of the same order of magnitude does well. $v = 0.1, 10^{-2}, 10^{-3}, 10^{-4}$, $m^2 = 10^{-3}$, $T \in [0.05, 0.1, 0.2, 0.3, 0.5, 0.7, 1.0, 1.3]$.

a scaling parameter is

$$\hat{T} := Tm^{2/3} \ln(1/v). \quad (39)$$

This collapses all curves on a single master curve, as shown in the main plot of Fig. 5.

We can go one step further. To do so, let us plot the \ln of f/f_c as a function of \hat{T}^ϕ . We find on Fig. 6 an almost linear behavior for an exponent $\phi = 0.55$, with slope -2.41 . Thus,

$$\frac{f}{f_c} \approx e^{-\left(\frac{\hat{T}}{\hat{T}_c}\right)^\phi}, \quad \phi \approx 0.55, \quad \hat{T}_c \approx 0.2, \quad (40)$$

is a stretched exponential. Note that if the fit is attempted close to $f \approx f_c$, then one can also conclude on $\phi \approx 0.51$. If we restrict to 10 percent deviation, then this allows for ϕ in the range $\phi \in [0.51, 0.56]$. We expect the regime $f/f_c \rightarrow 1$ to be governed by the depinning fixed point, and $f/f_c \rightarrow 0$

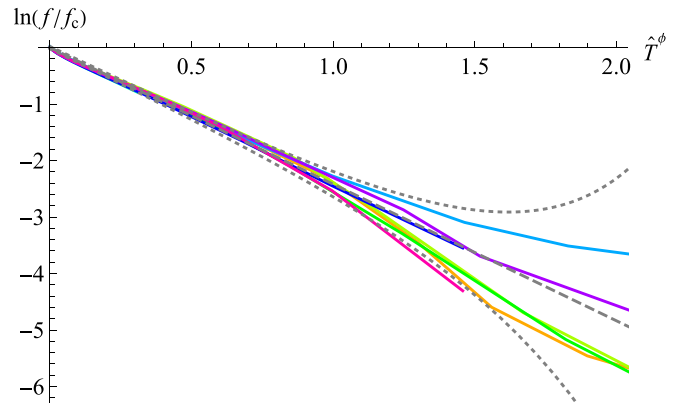


FIG. 6. This plot shows that as a function of temperature the scaled force f/f_c from Fig. 5 is a stretched exponential, with an exponent of $\phi \approx 0.55$. Gray dashed is a fit to a linear function, gray dotted putative error bars.

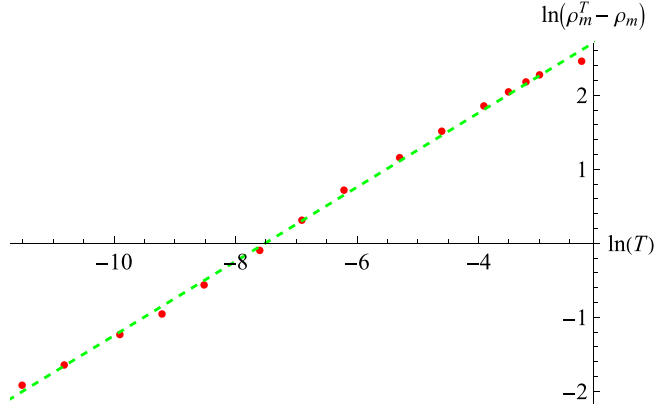


FIG. 7. Check of the scaling relation (41). The green dashed line has a slope of $\phi = 0.50$.

by the equilibrium fixed point. Thus, $f/f_c = 0.9$ is a small perturbation by temperature of the depinning fixed point, while $f/f_c = 0.1$ is a small perturbation of the equilibrium fixed point by a finite driving velocity. For $f/f_c \approx 1/2$ both effects are equally important.

Let us finally interpret \hat{T}_c : according to Eq. (39) $T = m^{-2/3} \hat{T}_c / \ln(1/v)$ is the temperature at which f/f_c is reduced by a factor of $1/e \approx 0.37$.

2. Correlation length as an order parameter

In Sec. II B 1 we established the mean force as an order parameter between equilibrium and depinning. While this is the most robust quantity we found, there are other quantities one may use. The first is the correlation length ρ_m , which decreases with temperature compared to its value at depinning. In the following, we denote by ρ_m the $T = 0$ value at depinning, and by ρ_m^T its finite-temperature value. If one considers zero-temperature depinning as a reference point, then at small temperatures

$$\rho_m - \rho_m^T \sim \hat{T}^\phi, \quad (41)$$

with $\phi = 0.50 \pm 0.02$; see Fig. 7.

3. Disorder amplitude as an order parameter

Assuming that

$$\Delta_{v,T}(w) = m^4 (\rho_m^T)^2 \tilde{\Delta}(w/\rho_m^T), \quad (42)$$

the amplitude $\Delta_{v,T}(0)$ at small T should behave as

$$\frac{\Delta_{v,T}(0)}{\Delta(0)} - 1 \simeq \left(\frac{\rho_m^T}{\rho_m} \right)^2 - 1 \sim T^\phi + \mathcal{O}(T^{2\phi}). \quad (43)$$

Our measurements presented in the inset of Fig. 8 are consistent with an exponent in the range $\phi \in [0.5, 0.6]$.

4. Disorder integral as an order parameter

Both the correlation length as well as the amplitude are very sensitive to details of the rounding around the cusp. More robust is the area under $\Delta(w)$. The above relations imply that

$$\frac{\int_{w>0} \Delta_{v,T}(w)}{\int_{w>0} \Delta(w)} \sim \left(\frac{\rho_m^T}{\rho_m} \right)^3 \sim T^\phi + \mathcal{O}(T^{2\phi}). \quad (44)$$

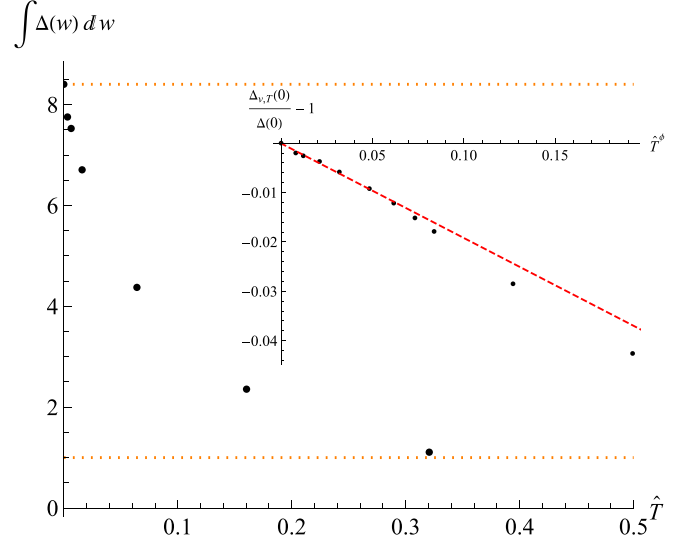


FIG. 8. Change with temperature of the area (main plot) and amplitude at $w = 0$ (inset) for $\phi = 0.56$.

Our data are consistent with an exponent in the range of $\phi = 0.5$ to $\phi = 0.67$, favoring the upper end. The decrease of the area is shown in Fig. 8. The orange dashed lines are references for depinning (top) and equilibrium (bottom).

C. Scaling close to equilibrium and depinning

Let us next consider scaling close to equilibrium and depinning.

1. Scaling near equilibrium

For equilibrium

$$\Delta(w) \sim m^{4/3} \tilde{\Delta}(wm^{4/3}). \quad (45)$$

While this scaling holds for all w at the zero-temperature fixed point, the scaling within the boundary layer is more subtle. Consider first the inset of Fig. 9. In black is shown the equilibrium fixed point for $m^2 = 0.1$; red/blue/purple show from top to bottom $m^2 = 0.1, 0.05, 0.01$ for $T = 1$, $v = 10^{-3}$. In the main plot we perform a scaling collapse from $m^2 = 0.01$ onto $m^2 = 0.1$. In blue dotted (marked as I), we rescaled by accounting for the difference in mass, i.e., with $m^{4/3}$. One sees that no scaling collapse is achieved. To improve the scaling collapse, one also needs to scale temperature with its corresponding dimension, i.e., $Tm^{-\theta}$ with $\theta = 2/3$, leading to the blue-dashed curve (marked as II). The remaining offset comes from the velocity which scales as m^2 . Using that $z = 2$ both in the free theory and at depinning, suggest a scaling of $v \sim m^{2/3}$. A look at the size of the boundary layer of the thermal peak suggests that the driving velocity should be reduced by a factor of 2, which is approximately consistent with the above scaling.

2. Scaling near depinning

In Figs. 10 and 11 we show the whole crossover regime from depinning to equilibrium. The previous section studied the change in correlation length and area as an order

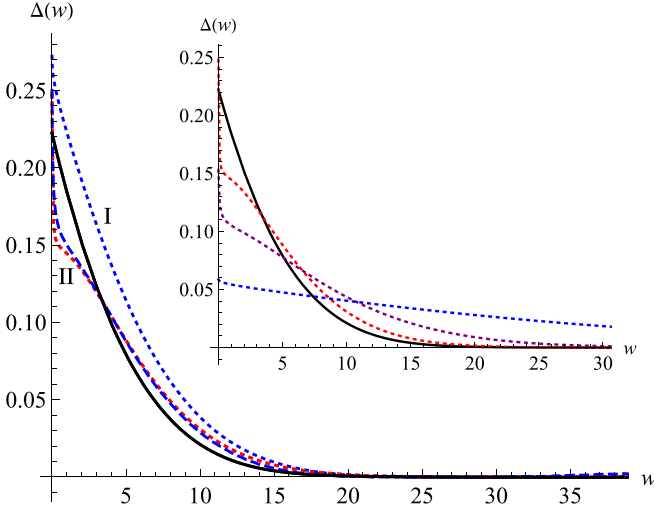


FIG. 9. Scaling of $\Delta(w)$ (DNS). The inset shows the equilibrium fixed point (EM) at $m^2 = 0.1$ (black) and $\Delta_{v,T}(w)$ for $m^2 = 0.1$ (red), $m^2 = 0.05$ (purple), and $m^2 = 0.01$ (blue) for $T = 1$, $v = 10^{-3}$. The main plot shows the collapse of $m^2 = 0.01$ onto $m^2 = 0.1$ (marked as I) rescaling only the explicit m -dependence. This is improved by rescaling in addition T as Tm^θ (marked as II).

parameter, but more can be said close to depinning. For this consider Fig. 10, at $v = 0.001$. In the inset we use the scaling relation (42) to collapse the curve for $T = 0.02$ onto the one for $T = 0$. In particular, this implies that the shape $\hat{\Delta}(w)$ is not affected by temperature. When comparing experimental

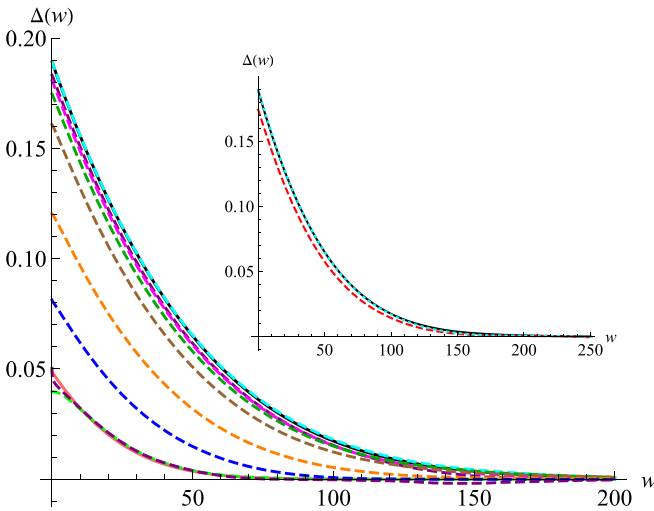


FIG. 10. Simulations (DNS) of $\Delta_{v,T}(w)$ for $m^2 = 0.01$, $v = 10^{-3}$ and $T \in [0, 0.005, 0.01, 0.02, 0.05, 0.2, 0.5, 1]$ from depinning (cyan-dashed, top) to the equilibrium regime (purple, bottom). Also shown are $v = 0$, $T = 0$ equilibrium fixed point (red, bottom EM), and the equilibrium thermal rounding (green). The inset shows a scaling collapse using the scaling relation in Eqs. (42) and (39) for $T = 0.02$, where $Tm^\theta \ln 1/v = 0.03$ is close to depinning. Brown dashed curve (main plot, $T = 0.05$, with $\Delta(0) = 0.16$) corresponds to $Tm^\theta \ln 1/v = 0.075$ already at 60 % of the maximal value of f_c . (see Fig. 5). No scaling collapse could be obtained here (red curve in the inset).

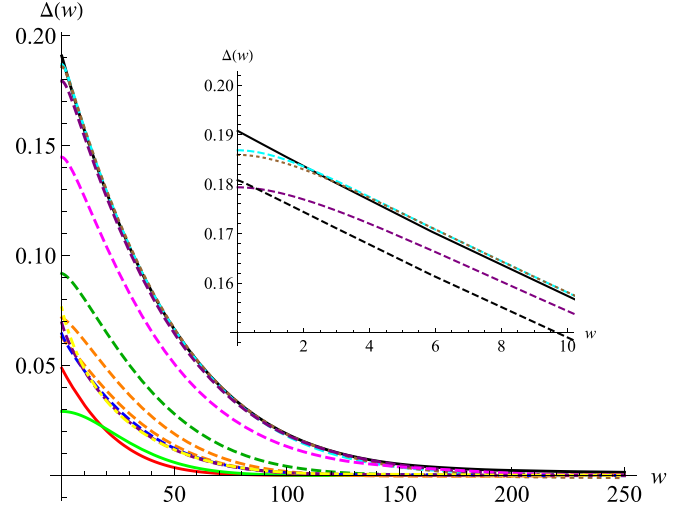


FIG. 11. $\Delta_{v,T}(w)$ (DNS) for $m^2 = 0.01$ at fixed $v = 0.1$ and varying T compared to the depinning (black, top) and equilibrium (red, bottom, EM) and thermal rounding at $T = 5$. From top to bottom temperature increases $T \in [0, 0.001, 0.01, 0.1, 0.5, 1, 2, 3, 4, 5]$. At $T = 3$, the velocity boundary layer disappears due to the formation of the thermal peak. Inset shows the small temperature effect on the boundary layer. It is little affected at small $T = 0.001$. Inset black dashed shows $T = 0.01$, $v = 10^{-3}$ and purple dashed $T = 0.01$, $v = 10^{-3}$, showing they are not related by velocity deconvolution.

data to theoretical predictions, this is important as scales are fixed using the correlation length. At larger T this no longer holds true, and the shape changes. Another interesting feature can be identified at a larger driving velocity. Consider Fig. 11 for $v = 0.1$, where rounding due to a finite driving velocity is clearly present. As we now know that when approaching equilibrium a thermal peak forms, one would expect some interplay between the velocity boundary layer and the thermal peak. Figure 11 shows that this is indeed the case. For large $T > 3$ an apparent cusp seems to re-emerge. Its nature, however, is very different from the cusps of the depinning and equilibrium fixed points. There it is related to the existence of shocks and avalanches. Here, it is an artifact of the combined effect of the velocity boundary layer and the thermal peak forming on top. This regime corresponds to $\hat{T} = 0.32$, which is far in the crossover regime of Fig. 5.

III. SUMMARY AND DISCUSSION

In this work we addressed the long-standing question of the full crossover between depinning and equilibrium. Studying the mean effective force and its correlator for a one-particle model, we characterized the phase diagram of finite velocity v and finite temperature T . This may serve as a reference point for experiments and simulations in dimensions $d > 0$. We showed that the mean force, divided by the mean force at depinning, is a robust order parameter, allowing one to quantify where one is in between depinning and equilibrium, and what one should expect for the force correlations.

Our results are directly applicable to the unzipping of a DNA hairpin [12]. This experiment has all the ingredients

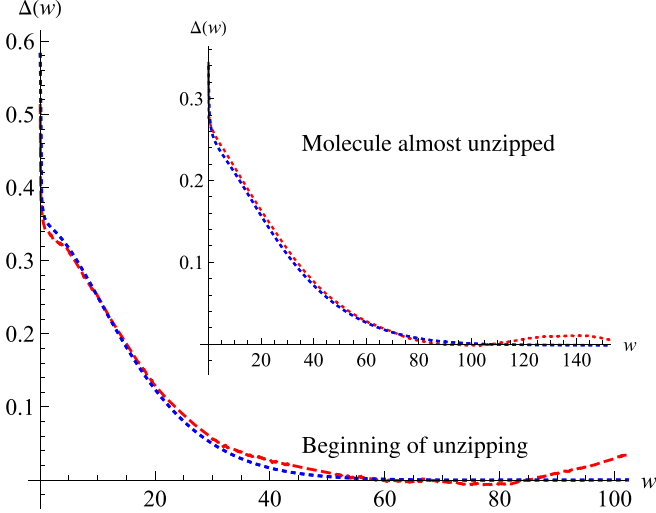


FIG. 12. Comparison of the experimental curve (red) to simulation (blue). For the main plot, simulation parameters are chosen to agree with the largest mass, i.e., small w in Eq. (46). In the inset we see results when the DNA molecule is almost unzipped, corresponding to a reduction in m by a factor of about 0.4. Again the simulation agrees well with the experiment, and captures the shape of the boundary layer.

studied here: It has a finite temperature, it has random forces, and it has a confining potential whose minimum is slowly increasing at a driving velocity v , allowing us to measure its force correlations. Earlier analysis [23] has suggested this experiment to be close to equilibrium. Interestingly, in this experiment the stiffness of the trap, (m^2 in our notation) decreases when unzipping the DNA molecule,

$$\frac{1}{m^2} = \frac{1}{m_0^2} + an = \frac{1}{m_0^2} + a'w, \quad (46)$$

where n is the number of unzipped bases, itself proportional to the position of the confining potential w , starting with $w = 0$ for the completely closed molecule. Reminding that m sets the renormalization scale, we see that the experiment runs the renormalization group for us! Figure 12 shows a comparison of experimental data for two different masses to numerical simulations. For the largest mass, simulation parameters are chosen such as to agree with experimental data. Using the ratio of masses in the experiment, this then predicts the simulation parameters for the smaller mass. We see that simulation and experiment agree well. Details can be found in Ref. [12].

We hope that this work serves as a reference where both the driving velocity v and temperature T are nonvanishing, and it is a priori not clear where in the phase diagram one is sitting. Looking at the measured critical force divided by its value at depinning allows one to identify where in the phase diagram an experiment is located. One can then assess and quantify all the features discussed here: Thermal rounding, the thermal peak and its broadening as a function of m^2 , as well as the scaling length ρ_m in the w direction. This should be useful to bring some order into these many-parameter systems.

ACKNOWLEDGMENTS

We thank A. Kolton and A. Rosso for sharing their experience, and P. Rissone, M. Rico-Pasto, and F. Ritort for the experimental collaboration on DNA unzipping.

APPENDIX A: NUMERICAL IMPLEMENTATIONS

The number of samples is denoted by N . In this work we use two numerical implementations:

(i) *Direct numerical simulation (DNS)*. To solve the coupled set of differential equations (7)–(10) we use a space discretization $\delta u = 10^{-2}$ to first obtain the random forces $F(u)$ for $u = n\delta u$, $n \in \mathbb{N}$. $F(u)$ is then linearly interpolated between these points. We finally solve Eq. (7) with the Euler method, using a time-discretization of $\delta t = 10^{-3}$.

(ii) *Exact minimization (EM)*. In the statics at temperature $T = 0$, the relevant quantities are computed using minimization of the energy in Eq. (15). For a given disorder realization $V(u)$, the minimum of the potential as a function of w is

$$\hat{V}(w) = \min_u \left[V(u) + \frac{m^2}{2}(u - w)^2 \right]. \quad (A1)$$

At finite temperature, this is replaced by

$$\hat{V}(w) = V(w) - T \ln \left(\left\langle e^{-\frac{V(u)-V(w)}{T} - \frac{m^2}{2T}(u-w)^2} \right\rangle_u \right). \quad (A2)$$

Using potential differences allows to better restrict the necessary range in $u - w$. For RF disorder, as for OU forces, the (microscopic) potential is obtained by integrating the random forces,

$$V(u) - V(w) = - \int_w^u F(u') du'. \quad (A3)$$

The effective force $\hat{F}(w) = -\partial_w \hat{V}$ then becomes

$$\hat{F}(w) = m^2 \frac{\left\langle e^{-\frac{V(u)-V(w)}{T} - \frac{m^2}{2T}(u-w)^2} (u - w) \right\rangle_u}{\left\langle e^{-\frac{V(u)-V(w)}{T} - \frac{m^2}{2T}(u-w)^2} \right\rangle_u}. \quad (A4)$$

APPENDIX B: BOUNDARY LAYER

At finite temperature, the unrescaled 1-loop FRG equation acquires an additional term,

$$-m\partial_m \Delta(w) = -\frac{1}{2} \partial_w^2 [\Delta(w) - \Delta(0)]^2 + \tilde{T}_m \Delta_m''(w) \dots \quad (B1)$$

$$\tilde{T}_m := 2Tm^\theta \int_k \frac{1}{k^2 + m^2} \Big|_{m=1}. \quad (B2)$$

(In dimension $d = 0$, the integral simplifies to $1/m^2$.) The fixed-point equation for the rescaled dimensionless disorder $\tilde{\Delta}(w) := m^{\varepsilon-2\zeta} \Delta(wm^\zeta)$ then takes the form

$$\begin{aligned} -m\partial_m \tilde{\Delta}(w) &= (\varepsilon - 2\zeta) \tilde{\Delta}(w) + \zeta w \tilde{\Delta}'(w) \\ &\quad - \frac{1}{2} \partial_w^2 [\tilde{\Delta}(w) - \tilde{\Delta}(0)]^2 + \tilde{T}_m \tilde{\Delta}''(w) \dots \end{aligned} \quad (B3)$$

What is remarkable about Eq. (B1) is that the RG flow conserves the integral $\int_{w>0} \Delta(w)$, both at vanishing temperature $\tilde{T}_m = 0$ and at $\tilde{T}_m > 0$. The reason is that the right-hand side of Eq. (B1) is a total derivative.

For the random-field solution $\zeta = \varepsilon/3$ in equilibrium, relevant for us, this also holds for the rescaled Eq. (B3).

The finite-temperature solution in the standard boundary-layer form is [15]

$$\Delta_T(w) \approx \mathcal{A}_T \Delta(\sqrt{w^2 + t^2}), \quad (\text{B4})$$

$$t = \frac{6Tm^2}{\varepsilon|\Delta'(0^+)|} \Leftrightarrow \frac{t}{\rho_m} = \frac{6Tm^2}{\varepsilon\Delta(0)}. \quad (\text{B5})$$

As the flow preserves the area, it is important to fix \mathcal{A}_T , such that the integrals on both sides coincide. This adds a nontrivial change in normalization which cannot be given in closed form. Another problem of the boundary layer is that given $\Delta_T(w)$, one can reconstruct $\Delta(w)$ only for $w \geq t$. Since the boundary layer is phenomenological and not exact, we propose a different approximation: namely, to obtain the finite- t solution by convoluting the zero-temperature solution with an appropriately chosen diffusion kernel,

$$\Delta_T(w) = \int_{-\infty}^{\infty} du \Delta(u) G(u - w, \tau), \quad (\text{B6})$$

$$G(u, \tau) = \frac{1}{\sqrt{4\pi\tau}} e^{-\frac{u^2}{4\tau}}. \quad (\text{B7})$$

A nice property of the convolution in Eq. (B6) is that by construction it is area preserving, thus no additional normalization \mathcal{A}_T is necessary. While using the diffusion kernel is natural, given that Eq. (B3) is the diffusion equation in absence of nonlinear terms, what remains to be done is to fix the “diffusion time” τ . Given the properties of the diffusion kernel, this can analytically be done for

$$\Delta(w) = \mathcal{C} e^{-w/\rho_m - b(w/\rho_m)^2}. \quad (\text{B8})$$

Demanding that $\Delta_T''(0)/\Delta_T(0)$ agree yields

$$\tau = \frac{t^2}{\pi} - \frac{2(\pi - 2)t^3}{\rho_m \pi^2} + \mathcal{O}(t^4). \quad (\text{B9})$$

The leading-order term only depends on t , while the subleading one contains ρ_m . Higher-order terms depend on the fitting parameter b in Eq. (B8).

Figure 13 shows a comparison of numerics for $m^2 = 0.01$ at $T = 0$ (black) and $T = 1$ (cyan) to the boundary-layer approximation (B4) (dark-green dot-dashed) and the diffusion kernel (B6) (red dashed), with t from Eq. (B5). Both approximations seem to work well.

APPENDIX C: EXACT RELATION BETWEEN MICROSCOPICS AND MACROSCOPICS

The FRG equation (B1) predicts that the integral $\int \Delta(w) dw$ remains unrenormalized. Therefore the integral over the microscopic disorder $\Delta_0(w)$ equals the integral over the renormalized disorder $\Delta(w)$, which we can rewrite through its scaling form (5) as

$$\begin{aligned} \int_0^\infty dw \Delta_0(w) &\equiv \int_0^\infty dw \Delta(w) \\ &= \int_0^\infty dw m^4 \rho_m^2 \tilde{\Delta}(w/\rho_m) \\ &= m^4 \rho_m^3 \int_0^\infty dw \tilde{\Delta}(w). \end{aligned} \quad (\text{C1})$$

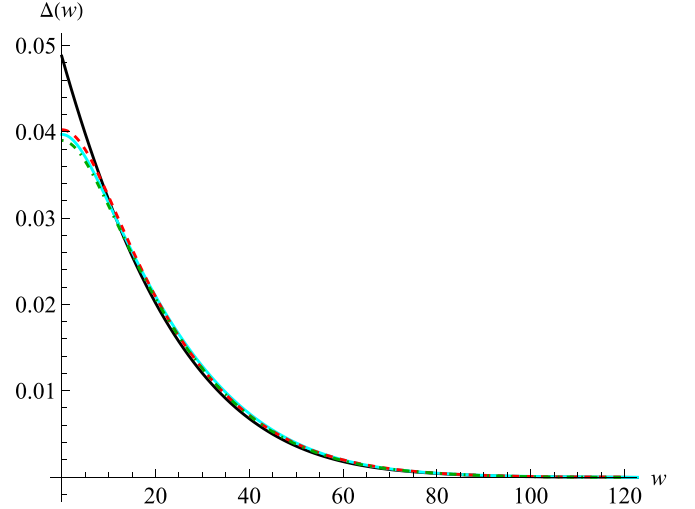


FIG. 13. Comparison of the boundary layer (dark-green dot-dashed) to the diffusion kernel (red-dashed), experimental data at $T = 1, m^2 = 0.01$ in cyan and the zero temperature fixed point in black.

Since $\rho_m \sim m^{-\zeta}$, the combination $m^4 \rho_m^3$ is independent of m for RF disorder which has $\zeta = 4/3$. (Note that this also works in dimension $d > 0$, with m^4 in Eq. (C1) replaced by m^ε , $\varepsilon = 4 - d$, and $\zeta = \varepsilon/3$.) Solving for ρ_m we find

$$\rho_m = \left[\frac{\int_{w>0} \Delta_0(w)}{m^4 \int_{w>0} \tilde{\Delta}(w)} \right]^{1/3}. \quad (\text{C2})$$

For equilibrium RF disorder in $d = 0$ (see Sec. IC1), $\int_{w>0} \tilde{\Delta}(w) = 0.252$, and this reduces to

$$\rho_m = \left[\frac{3.97}{m^4} \int_{w>0} \Delta_0(w) \right]^{1/3}. \quad (\text{C3})$$

Equation (C1) has been verified experimentally in Ref. [12]. Here we perform a numerical test. For the simulations of Fig. 2 microscopic forces are taken constant on an interval of size one, with variance 1. As a consequence, the microscopic disorder has integral $\int_{w>0} \Delta_0(w) = 1/2$. Numerical simulations of Eq. (15) confirm that this is preserved under RG: $\int_{w>0} \Delta(w) = 0.496$ for $m^2 = 10^{-2}$, $\int_{w>0} \Delta(w)w = 0.484$ for $m^2 = 10^{-3}$, and $\int_{w>0} \Delta(w) = 0.525$ for $m^2 = 10^{-4}$. Using Eq. (C3) this gives a prediction for the scale ρ_m . This confirms for a single particle that if the microscopic disorder is known, then there are no unknown scales. Both ρ_m as well as $\Delta(0)$ are predicted by the microscopic disorder.

APPENDIX D: NOTATIONS

Our study contains the depinning fixed point at scale m , which when properly rescaled is close to its $m \rightarrow 0$ limit. It further contains two relevant perturbations away from it: temperature T and driving velocity v . This leads to different observables and their rescaled versions, summarized here:

(1) m^2 is the strength of the confining potential, which sets the overall (renormalization) scale.

(2) $u(t)$ is the interface position as a function of time t , u_w the interface position given a minimum for the confining potential at $u = w$. We mostly use this in the limit of $v \rightarrow 0$, where the former cannot be defined.

(3) F_w is the force seen by the confining potential positioned at w , defined in Eq. (11). It depends on m and v, T .

(4) f_c is the critical/pinning force in the limit of $T \rightarrow 0$ (first) and $v \rightarrow 0$ (second), defined in Eq. (12). It still depends on m , but converges quickly when $m \rightarrow 0$ [24].

(5) f , defined in Eq. (37), is the measured pinning force. $f = f_c$ at depinning and $f = 0$ in equilibrium.

(6) $\Delta_{v,T}(w)$ is the measured $v > 0, T > 0$ effective force correlator defined in Eq. (13).

(7) $\Delta(w)$ is the effective force correlator defined in Eq. (16) for equilibrium (Sinai) and Eq. (26) for depinning (Gumbel class).

(8) $\tilde{\Delta}(w)$ is the rescaled force correlator, defined in Eq. (18) for equilibrium and Eq. (27) for depinning.

(9) $\Delta_T^{\text{eq}}(w) = \Delta_T(w)$ is the zero-velocity, thermally rounded equilibrium force correlator defined in Eq. (19).

(10) $\Delta_v^{\text{TP}}(w)$ is the thermal peak defined in Eq. (33).

-
- [1] H. Barkhausen, Zwei mit Hilfe der neuen Verstärker entdeckte Erscheinungen, *Phys. Ztschr.* **20**, 401 (1919).
 - [2] G. Durin, F. Bohn, M. A. Correa, R. L. Sommer, P. Le Doussal, and K. J. Wiese, Quantitative scaling of magnetic avalanches, *Phys. Rev. Lett.* **117**, 087201 (2016).
 - [3] P. Cizeau, S. Zapperi, G. Durin, and H. Stanley, Dynamics of a ferromagnetic domain wall and the Barkhausen effect, *Phys. Rev. Lett.* **79**, 4669 (1997).
 - [4] C. ter Burg, F. Bohn, F. Durin, R. L. Sommer, and K. J. Wiese, Force correlations in disordered magnets, *Phys. Rev. Lett.* **129**, 107205 (2022).
 - [5] P. Le Doussal, K. J. Wiese, S. Moulinet, and E. Rolley, Height fluctuations of a contact line: A direct measurement of the renormalized disorder correlator, *Europhys. Lett.* **87**, 56001 (2009).
 - [6] B. Gutenberg and C. F. Richter, Frequency of earthquakes in California, *Bull. Seismol. Soc. Am.* **34**, 185 (1944).
 - [7] B. Gutenberg and C. F. Richter, Earthquake magnitude, intensity, energy, and acceleration, *Bull. Seismol. Soc. Am.* **46**, 105 (1956).
 - [8] K. J. Wiese, M. Bercy, L. Melkonyan, and T. Bizebard, Universal force correlations in an RNA-DNA unzipping experiment, *Phys. Rev. Res.* **2**, 043385 (2020).
 - [9] P. Le Doussal and K. J. Wiese, How to measure Functional RG fixed-point functions for dynamics and at depinning, *Europhys. Lett.* **77**, 66001 (2007).
 - [10] A. A. Middleton, P. Le Doussal, and K. J. Wiese, Measuring functional renormalization group fixed-point functions for pinned manifolds, *Phys. Rev. Lett.* **98**, 155701 (2007).
 - [11] A. Rosso, P. Le Doussal, and K. J. Wiese, Numerical calculation of the functional renormalization group fixed-point functions at the depinning transition, *Phys. Rev. B* **75**, 220201(R) (2007).
 - [12] C. A. ter Burg, P. Rissone, M. Rico-Pasto, R. Ritort, and K. Wiese, Experimental test of Sinai's model in DNA unzipping, *Phys. Rev. Lett.* **130**, 208401 (2023).
 - [13] C. ter Burg and K. J. Wiese, Mean-field theories for depinning and their experimental signatures, *Phys. Rev. E* **103**, 052114 (2021).
 - [14] L. Balents and P. Le Doussal, Thermal fluctuations in pinned elastic systems: Field theory of rare events and droplets, *Ann. Phys. (NY)* **315**, 213 (2005).
 - [15] K. J. Wiese, Theory and experiments for disordered elastic manifolds, depinning, avalanches, and sandpiles, *Rep. Prog. Phys.* **85**, 086502 (2022).
 - [16] B. Alessandro, C. Beatrice, G. Bertotti, and A. Montorsi, Domain-wall dynamics and Barkhausen effect in metallic ferromagnetic materials. I. Theory, *J. Appl. Phys.* **68**, 2901 (1990).
 - [17] B. Alessandro, C. Beatrice, G. Bertotti, and A. Montorsi, Domain-wall dynamics and Barkhausen effect in metallic ferromagnetic materials. II. Experiments, *J. Appl. Phys.* **68**, 2908 (1990).
 - [18] P. Le Doussal and K. J. Wiese, Avalanche dynamics of elastic interfaces, *Phys. Rev. E* **88**, 022106 (2013).
 - [19] A. A. Middleton, Asymptotic uniqueness of the sliding state for charge-density waves, *Phys. Rev. Lett.* **68**, 670 (1992).
 - [20] Y. G. Sinai, The limiting behaviour of a one-dimensional random walk in a random environments, *Theory Probab. Appl.* **27**, 256 (1983).
 - [21] P. Le Doussal, Exact results and open questions in first principle functional RG, *Ann. Phys.* **325**, 49 (2010).
 - [22] P. Le Doussal and K. J. Wiese, Driven particle in a random landscape: Disorder correlator, avalanche distribution and extreme value statistics of records, *Phys. Rev. E* **79**, 051105 (2009).
 - [23] J. M. Huguët, N. Forns, and F. Ritort, Statistical properties of metastable intermediates in DNA unzipping, *Phys. Rev. Lett.* **103**, 248106 (2009).
 - [24] M. N. Semeikin and K. J. Wiese, Roughness and critical force for depinning at 3-loop order, *Phys. Rev. B* **109**, 134203 (2024).